ELECTRON CLOUD AND SINGLE-BUNCH INSTABILITIES IN THE RELATIVISTIC HEAVY ION COLLIDER*

J. Wei† [1], M. Bai[1], M. Blaskiewicz[1], P. Cameron[1], R. Connolly[1], A. Della Penna[1]
W. Fischer[1], H.C. Hseuh[1], H. Huang[1], U. Iriso[3], R. Lee[1], R. Michnoff[1]
V. Ptitsin[1], T. Roser[1], T. Satogata[1], S. Tepikian[1], L. Wang[2], S.Y. Zhang[1]
Collider-Accelerator Department, Brookhaven National Laboratory, Upton, New York, USA[1]
Stanford Linear Accelerator Center, California, USA[2]; CELLS, Bellaterra, Spain[3]

Abstract

Electron cloud is a leading mechanism limiting RHIC intensity upgrades. Electron cloud in RHIC is in an intermediate regime sharing features of both the long-bunch (PSR) and short-bunch (photon factories) machines. Vacuum-pressure rises, transverse tune shifts, and electron flux are observed at injection, upon transition crossing, and at top energy. Transverse emittance growth, fast instabilities, and beam loss also occur upon transition crossing. Mitigation measures are implemented both to reduce the production of electron cloud and to control the beam stability.

INTRODUCTION

Since the first reports four decades ago [1]-[5], electron-cloud effects are found to limit the performance of many high-intensity and high-brightness circular accelerators [6]. A fast, transverse electron-proton instability and the induced beam loss limits the beam intensity in the Proton Storage Ring (PSR) at the Los Alamos National Laboratory (LANL) [7]. Transverse emittance blow-ups caused by the e-cloud limit the luminosity in the lepton factories (BEPC, KEKB, PEP-II) [8]-[11]. During operations of the Relativistic Heavy Ion Collider (RHIC), vacuum-pressure rises associated with electron-induced gas desorption are found to limit the number of stored bunches and the beam intensity [12]-[14]. Electron-cloud phenomena include transverse tune shifts (KEKB, AGS Booster, RHIC), coupled-bunch (B factories, BEPC, PS, SPS) and single-bunch (KEKB, SPS, PSR, RHIC) instabilities, vacuum-pressure rise (RHIC etc.), emittance growth (KEKB, PEP-II, SPS, RHIC), beam diagnostics interference (RHIC, PS, SPS, PSR), and heat load on superconducting cryogenic wall (SPS beam experiments).

This paper mainly discusses e-cloud-induced instability effects in RHIC. We review key mechanisms of e-cloud formation, and summarize experimental observations and mitigation measures.

MECHANISM

Key mechanisms pertaining to the formation of electron cloud are beam-driven electron multipacting and electron trapping. Depending on the beam parameters, the multipacting can be classified into several regimes: multiple short-bunch multipacting [4, 15, 16, 17], single long-bunch, trailing-edge multipacting [7, 18], and the intermediate regime. For the long-bunch and dc-beam [2, 3] cases, beam-induced trapping is critical to sustain electron concentration. For the short-bunch cases, trapping due to magnetic field is suspected to be responsible for the long electron lifetime over beam gaps [19].

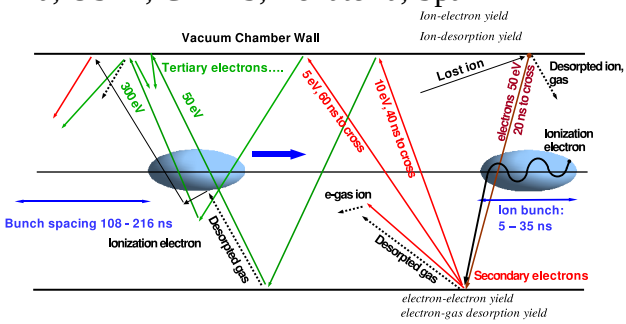

Figure 1: Electron build-up due to intermediate-regime beam-induced multipacting. The time between successive bunches is typically 108 ns when the multipacting occurs. The energy gain due to bunch passage is up to 500 eV.

RHIC belongs to the intermediate regime where the transit time of the electrons crossing the vacuum pipe is comparable to the bunch length, as shown in Fig. 1. Between the subsequent bunches, the electrons typically reflect from the vacuum chamber wall for several times. Upon acceleration by the beam bunch, the electrons gain energy up to several hundred eV, and hit the wall with an average SEY $Y_{ee,0}$ typically much larger than 1 (Fig. 2). Upon subsequent impacts on the wall, the electron energy is low (typically below 10 eV) due to lack of beam potential, and the average secondary-emission yield $Y_{ee,i}$ ($i = 1, \ldots$) is smaller than 1. We define the characteristic SEY $Y_{ee,C}$ as the product of the average SEY of N_{ee} reflections between two subsequent bunch passage. The threshold for the multipacting in this regime corresponds to the condition when

$$Y_{ee,C} \equiv \Pi_{i=0,1,\ldots,N_{ee}} Y_{ee,i} > 1 \qquad (1)$$

where

$$Y_{ee,0} > 1, \text{ and } Y_{ee,i} < 1 \text{ for } i = 1, \ldots, N_{ee} \qquad (2)$$

Multipacting in the intermediate regime shares the features of both the short-bunch and long-bunch regimes. The build-up is not only sensitive to the bunch spacing and bunch pattern, but also sensitive to the bunch length and

* Work performed under the auspices of the US Department of Energy.
† jwei@bnl.gov

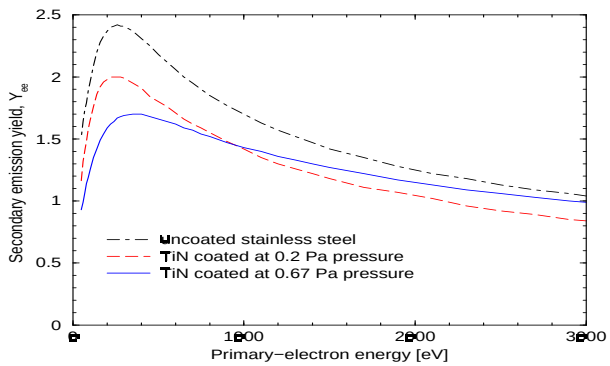

Figure 2: Examples of secondary-electron yield as a function of the incident electron energy for various surface conditions (courtesy P. He, N. Hilleret, H. Hseuh, R. Todd).

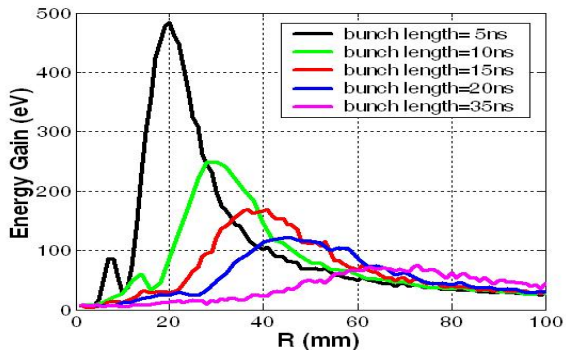

Figure 3: Electron's average energy gain as a function of its initial position R when it meets the follow-up bunches. The ion intensity corresponds to 10^{11} charges per bunch, and the transverse rms beam size is 2.4 mm.

peak density (Fig. 3). With a shorter bunch spacing, the number of low-energy electron passages N_{ee} is reduced, increasing the chance of exceeding multipacting threshold $Y_{ee,C} > 1$. With a shorter bunch length and higher peak beam density, the electron energy gain upon bunch acceleration becomes higher, leading to a higher secondary emission yield $Y_{ee,0}$ and $Y_{ee,C}$. Mechanisms that sustain electron concentration include reflections from the vacuum-chamber wall, trapping by the beam residual in the gap, trapping by the magnetic fields, and possible secondary ionization and trapping.

EXPERIMENTAL OBSERVATIONS

During typical operations, up to 57 ion bunches at 216 ns spacing, each containing about 10^{11} charges (e.g., 10^9 Au^{79+}, 5×10^9 Au^{79+}, or 10^{11} protons), are injected into each ring and accelerated to the top energy for hours of storage. During acceleration, the bunch length reaches the minimum, and the peak line density reaches the maximum when the beam crosses the transition energy.

In the following, we present RHIC observations in two categories: effects due to electron accumulation and electron-ion interaction including both bunch-train dependent and bunch trailing-edge phenomena.

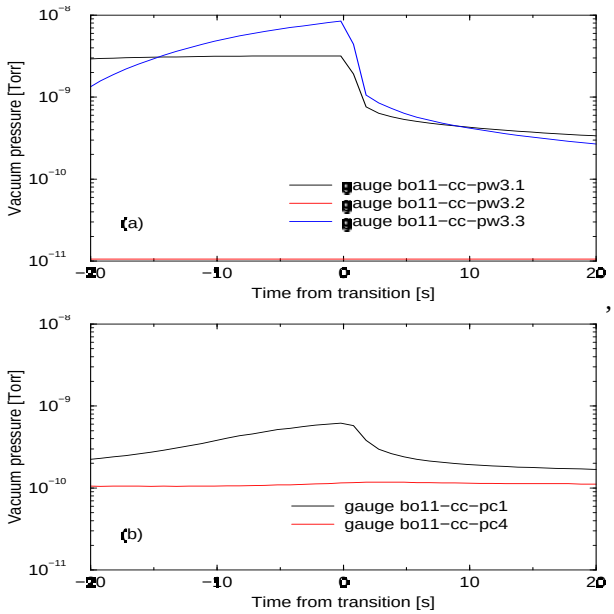

Figure 4: Effective vacuum pressure rise in the (a) warm and (b) cold region of the ring around transition crossing at time $t = 0$. Pressure on gauge bo11-cc-pw3.2 located between the two NEG-coated pipes does not rise.

Effects of Electron Accumulation

During typical operations, e-cloud does not noticeably affect the primary ion beam dynamics. Effects due to electron accumulation include vacuum pressure rise, experimental background, and instrumentation interferences.

Pressure rise often occurs in the interaction region (IR) where beams in the two rings are both present effectively doubling the local beam density; in regions where unbaked surfaces are exposed to the beam; in regions where high SEY material surfaces (e.g. Be chamber in the experimental region); when the bunch spacing is reduced to 108 ns; and upon transition crossing and rebucketing when the bunch peak density reaches the maximum (Fig. 4). In both the room-temperature (warm) and superconducting magnet (cold) regions, an increase of up to three orders of magnitude in the effective pressure is typically observed. Temperature rise is not observed at a resolution of about 0.01 K corresponding to a heat load of about 5 W per 100 m.

The vacuum pressure can be directly correlated with the integral electron flux on the wall measured by a retarding-field electron detector [14]. In addition to the beam-induced electron multipacting, beam-induced vacuum runaway caused by gas desorption from the pipe surface and subsequent ionization by the beam may also contribute to a pressure increase.

Effects of Electron-ion Interaction

During 2004 - 2005 studies, we created a simple machine condition to enhance the e-cloud while suppressing other irrelevant effects [20]. We inject ion beam only into one (blue) of the two rings with a bunch spacing of 108 ns.

While keeping the bunch intensity to the nominal (about 10^{11} charge), we keep the number of bunches to 40 to avoid uncontrollable pressure rise and beam loss. With only 1/3 of the ring occupied by the beam, the total beam intensity is also low (Table 1).

Table 1: RHIC parameters during year 2004 - 2005 electron-cloud studies.

Ring circumference	3833.8	m
Ring revolution period	12.79	μs
Aperture, IR (2/6/8/10, 4/12)	7, 12	cm
Aperture (arc, triplet)	7, 13	cm
Beam species	Cu^{29+}	
Energy, injection - top	9.8 - 100	GeV/u
Transition energy, γ_T	22.9	
Bunch intensity	5×10^9	
Bunch center spacing	108	ns
Bunch length at transition, full	$\sim$ 5	ns
Electron bounce frequency	$\sim$ 400	MHz
Peak bunch potential	$\sim$ 1.6	kV
e^- energy gain upon acceleration	$<$ 500	V

The ion beam motion is mostly susceptible to e-cloud impact at the time of transition crossing when the longitudinal motion is non-adiabatic. Instability is likely to occur due to lack of synchrotron oscillation and synchrotron frequency spread [21]. On a beam of 216 ns bunch spacing, most of the undesired effects (chromatic nonlinearity, self-field mismatch, and impedance-induced instabilities) near transition are mitigated by the γ_T-jump scheme during about 50 ms around the transition [21, 22], and all instabilities are cured by adjusting the timing and magnitude of the chromaticity jump, and the activation of octupole magnets [22]. However, these measures are not adequate for instability suppression when the bunch spacing is reduced to 108 ns.

Electron flux As the beam approaches transition, vacuum pressure-rise occurs during a time of seconds as the beam peak density increases (Fig. 4). Correspondingly, the peak value of the electron flux also increases. Fig. 5 shows the growth of the flux along the 40-bunch train at different times with respect to transition $t = 0$.

Beam loss Electron cloud impacts the beam mostly within about 0.1 s of transition crossing when the beam particle motion is non-adiabatic, causing electron-ion instabilities. With the accelerating voltage $V_{rf} = 300$ kV, beam losses are measured with the wall current monitor across γ_T varying from 13% for the first to 42% for the last bunch (Fig. 6). In comparison, at 216 ns spacing the loss is less than 5% uniform across the bunch train. Fig. 7 shows about 73% loss for bunch #40 with $V_{rf} = 300$ kV.

Transverse emittance growth Bunch-train dependent transverse emittance growth at γ_T is observed when the beam loss is moderate (Fig. 8). With a larger beam loss (e.g., $V_{rf} \geq$200 kV cases), the dependence becomes not

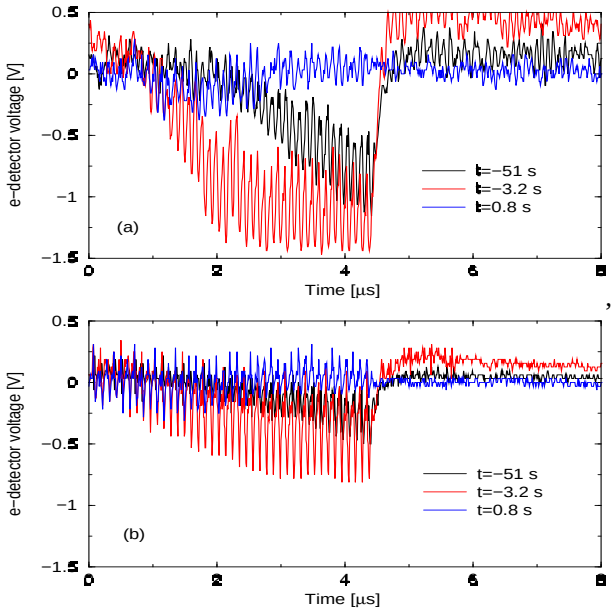

Figure 5: Electron flux measured in the (a) horizontal and (b) vertical directions near transition (γ_T) at $t = 0$. An ac-coupled amplifier is used with a low-frequency cut-off of about 300 kHz. The grid is not biased. The collector is biased at 50 - 100 V positive.

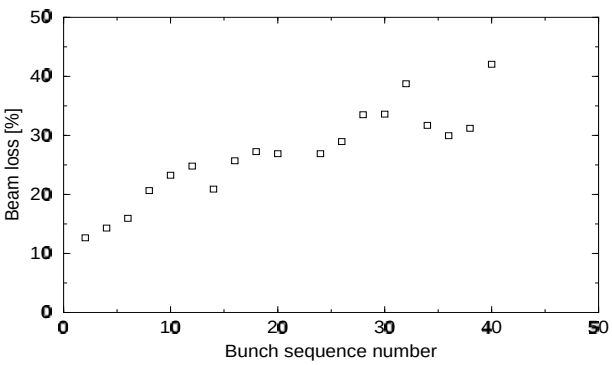

Figure 6: Beam loss at transition as a function of bunch sequence number with V_{rf}=200 kV and $b_{act} = -3$ unit. Major machine parameters are listed in Table 1.

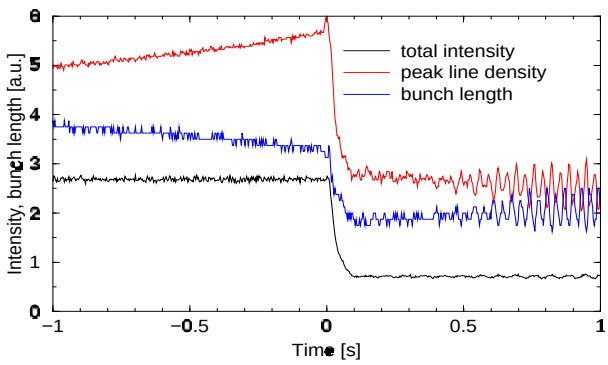

Figure 7: Beam loss and bunch size variation of bunch #40 near γ_T with $V_{rf} = 300$ kV and $b_{act} = -1$ unit. Total 40 bunches are injected with a spacing of 108 ns. Bunch train dependence of the beam loss is similar to Fig. 6.

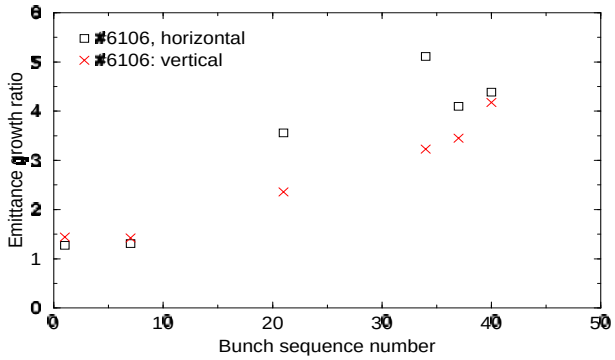

Figure 8: Bunch train dependence of the beam emittance growths at γ_T with V_{rf}=100 kV and $b_{set} = -1$ unit.

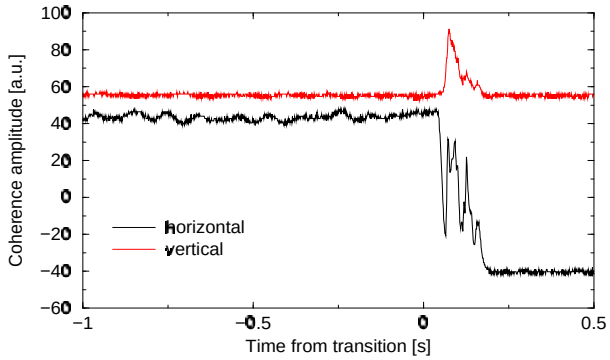

Figure 9: Coherence signal of bunch #40 from the turn-by-turn BPM data. The horizontal instability signal is within a step caused by the orbit shift due to γ_T-jump.

obvious, presumably because particles of larger emittance are lost. An accurate measurement is difficult with the ionization profile monitor when the loss-related pressure rise is excessive.

Transverse fast instability Fig. 9 shows the transverse coherence signal defined as the transverse centroid displacement measured from the turn-by-turn beam position monitor (BPM). A transverse instability occurs immediately after transition for about 0.1 s, leading to beam loss and emittance growth that are increasingly severe for later bunches of the bunch train. Fig. 10 shows the mean square of difference signal measured by a "button" BPM at 0.5 ns sampling rate. Again, the horizontal signal is complicated by the γ_T-jump induced orbit shift.

Tune shift Bunch-train dependent coherent tune shifts were observed during the injection of proton bunches at an intensity of 0.3×10^{11} per bunch and 108 ns bunch spacing. The tune shift of about 2.5×10^{-3} corresponds to an electron density of up to 2 nC/m [13]. Measurement of bunch-dependent tune shift during acceleration ramping is yet to be attempted.

Bunch trailing-edge phenomena Fig. 11 shows that beam loss near γ_T occurs mostly at the trailing edge of the bunch matching the e-cloud mechanism. Computer simulation (Fig. 12) shows that the electron density at the trailing

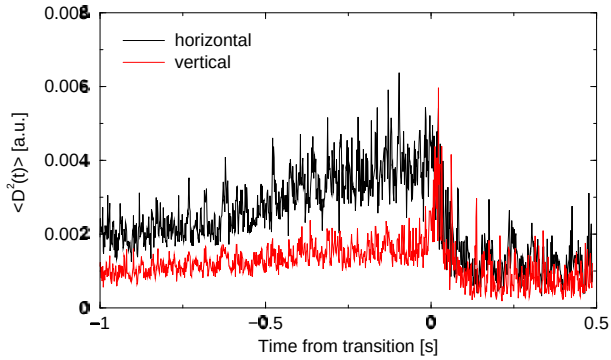

Figure 10: Mean square of the difference displacement measured by the "button" BPM sampling every 0.5 ns.

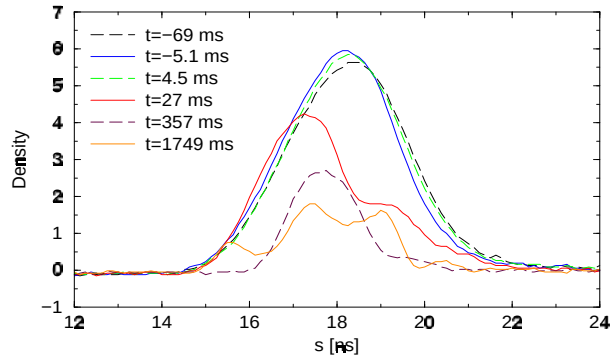

Figure 11: Evolution of the longitudinal profile upon the beam loss near γ_T with V_{rf}=300 kV and $b_{set} = -1$ unit.

edge of the bunch is about 3 times that at the rising edge. In the longitudinal direction, neither instability nor bunch-train dependent emittance growth are observed.

MITIGATION MEASURES

Control of the electron-cloud effects involves reducing the uncontrolled beam loss, suppressing electron generation, and enhancing Landau damping. The inner surface of the stainless-steel pipe in the RHIC warm region are being coated with non-evaporative getter (NEG) to lower

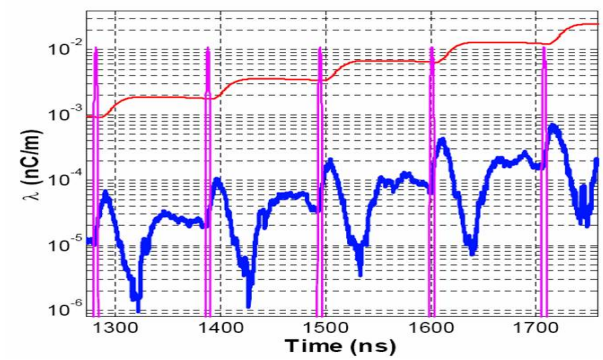

Figure 12: Simulation of the ion beam bunch longitudinal profile (purple), electron density in the vacuum pipe (red), and in the beam (blue) indicating the growth of e-cloud and the enhancement at the bunch trailing edge.

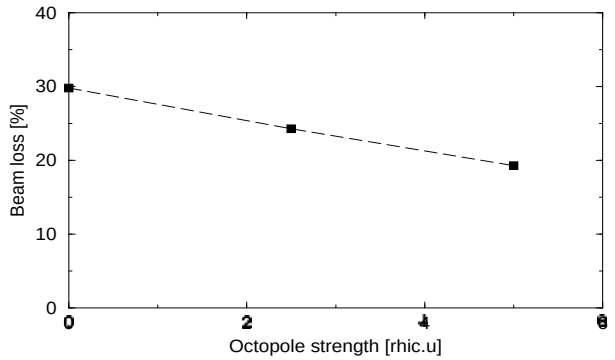

Figure 13: Average beam loss at γ_T as a function of the octopole magnet strength $|b_{oct}|$ with $V_{rf} = 300$ kV.

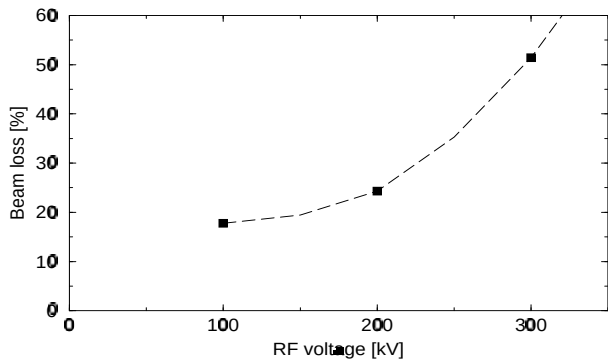

Figure 14: Average beam loss at γ_T as a function of the RF voltage with $b_{oct} = -3$ unit.

both the secondary emission and desorption yield, and to increase local vacuum pumping. Beam experiments confirmed the effectiveness of the coating in reducing the pressure rise (Fig. 4). Solenoidal fields applied in the warm section also reduces the pressure rise [14]. The cold region is pumped down to a pressure below 1×10^{-2} Torr before the cryogenic cool down to reduce the physi-sorbed gas to sub-monolayers [23].

During 2004 - 2005 studies, it is shown that beam loss induced by the transverse instability is modestly reduced by the damping by octupole families (Fig. 13), and dramatically reduced by lowering the RF voltage so that peak beam density, electron energy gain, and electron multipacting are all reduced. RF manipulation using multi-harmonic RF or induction RF is also explored (Fig. 14) [24].

DISCUSSIONS AND SUMMARY

Electron cloud is found to be a serious obstacle on the RHIC upgrade path. At a bunch spacing corresponding to twice the design number of bunches, electron accumulation and electron-ion interaction are found to cause transverse instabilities, emittance growth, and beam loss along with vacuum pressure rise during transition crossing.

Many questions remain to be answered. (1) It is not clear why the beam loss of the first bunch in the train is much higher than the nominal. More detailed logging of the vacuum pressure (every 0.1 s instead of 1 s) may clarify

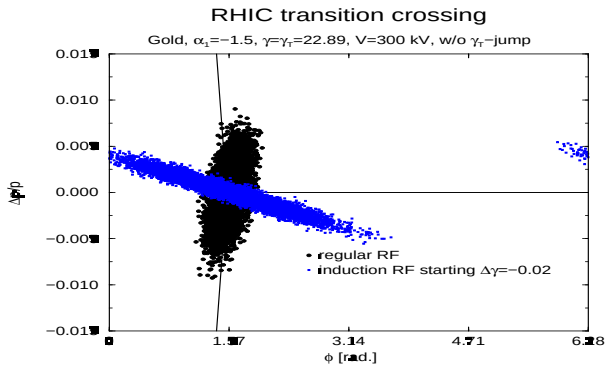

Figure 15: Longitudinal phase space showing the reduction of peak bunch density near γ_T using an induction RF system [24].

the gas scattering contribution. (2) It is not clear whether the instability alone causes more than 70% beam loss in 10 ms; what are the principle instability modes [25]; and why beam loss and the transverse instability occur only after but not before transition. A possible explanation yet to be verified is a sizable tune shift due to e-cloud coupled with a transition-jump lattice close to resonance. e-detector data needs to be logged in finer steps (1 ns instead of 10 ns) to explore e-cloud generation within each single bunch.

We thank R. Calaga, M. Furman, C. Montag, K. Ohmi, and F. Zimmermann for many helps and discussions.

REFERENCES

[1] G.I. Budker et al, Intern. Sym. Electron and Positron Storage Rings, Saclay (1966, Orsay, Univ. de France) VIII-6-1
[2] H. Hereward, CERN Report 71-15 (1971)
[3] E. Keil et al, CERN Report CERN-ISR-TH-71-58 (1971)
[4] A. Gröbner, 1977 Int. Conf. on High Energy Accel., Protvino (1977) 277
[5] D. Neuffer, et al, Nucl. Instru. Meth., **A321** (1992) 1
[6] J. Wei, Rev. Mod. Phys., **75** (2003) 1383
[7] R. Macek et al, PAC 01 (2001) 688
[8] F. Zimmermann, PAC 01 (2001) 666
[9] M. Izawa et al, Phys. Rev. Lett., **74**, (1995) 5044
[10] K. Ohmi, Phys. Rev. Lett., **75** (1995) 1526
[11] Z.Y. Guo et al, APAC 98 (1998) 432
[12] S.Y. Zhang, BNL note C-A/AP/67 (2001); EPAC (2004) 944
[13] W. Fischer et al, Phys. Rev. ST-AB, **5** (2002) 124401
[14] U. Iriso, et al, BNL note C-A/AP/129 (2003); ICFA BD News., **33** (2004) 128; BNL note C-A/AP/191 (2005)
[15] F. Zimmermann, LHC Report 95; SLAC-PUB-7425 (1997)
[16] M.A. Furman, KEK Proc. 97-17 (1997) 170
[17] F. Ruggiero et al, Phys. Rev. ST-AB, **2** (2001) 012801; Erratum **2** (2001) 029901
[18] V. Danilov et al, AIP Conf. Proc. 496, (1999) 315
[19] L. Wang, et al, Phys. Rev. ST-AB, **5** (2002) 124402; Phys. Rev. **E70** (2004) 036501
[20] J. Wei et al, CARE-HHH Workshop, CERN (2004); PAC 05 (2005) 4087
[21] J. Wei, Ph. D Thesis (1990, Stony Brook)
[22] C. Montag et al, PAC 03 (2003) 1702
[23] H. Hseuh, et al, ECLOUD 04 (Napa, 2004)
[24] K. Takayama et al, PAC 05 (2005) 4314
[25] M. Blaskiewicz et al, PAC 03 (2003) 3028